

Non-ionizing near-infrared radiation transillumination spectroscopy for breast tissue density and assessment of breast cancer risk

Michelle K. Simick*

University of Toronto
Department of Medical Biophysics
610 University Ave.
Toronto, Ontario M5G 2M9
Canada

Roberta Jong†

Mount Sinai Hospital
Toronto, Ontario M5G 2M9
Canada

Brian Wilson

Lothar Lilge

University of Toronto
Department of Medical Biophysics
610 University Ave.
Toronto, Ontario M5G 2M9
Canada
and
University Health Network
Toronto, Ontario
Canada
E-mail: llilge@uhnres.utoronto.ca

Abstract. There is increasing attention to prevention as a means to reduce cancer incidence. Prevention interventions or therapies in turn rely on risk assessment programs to identify those women most likely to benefit from education and lifestyle changes. These programs are usually based either on interviews to identify ethnic, genetic, and lifestyle factors contributing to risk or on physical examination of the breast. For the latter it has been shown that the parenchymal density pattern observed in X-ray mammography can be used to assess an individual's risk. Extensive areas of dense, glandular tissue that are relatively radio-opaque are associated with higher breast cancer risk, with an odds ratio of 4 to 6 compared with women in whom the breast density is low owing to an abundance of adipose tissue. Near-infrared optical transillumination spectroscopy has been used previously to investigate the physiological properties of breast tissue. In this study, women were recruited who underwent recently X-ray mammography. The tissue density was assessed by a radiologist. The women then underwent optical transillumination spectroscopy, for which an instrument was developed that delivered visible and near-infrared light to the breast. After being transmitted through the breast craniocaudally in one of four quadrants, the spectrum from 625 to 1050 nm was measured. The spectra were used as input to a Principal Component Analysis (PCA) that used the corresponding mammographic density as the reference standard. The study group consisted of 92 women aged 39 to 72 years. Without further stratification for age, menopausal status, or measurement position, the PCA numerical model predicted the radiological assessment of tissue density in the mid 80% to low 90%. © 2004 Society of Photo-Optical Instrumentation Engineers. [DOI: 10.1117/1.1758269]

Keywords: cancer risk, transillumination spectroscopy, breast cancer, cancer prevention.

Paper 03059 received May 7, 2003; revised manuscript received Sep. 29, 2003; accepted for publication Oct. 23, 2003.

1 Introduction

Breast cancer is the most commonly occurring cancer in women. In Canada, the lifetime risk of being diagnosed with breast cancer is approximately 1 in 10,¹ the highest out of all cancers for women. The probability of dying of breast cancer is 1 in 25, which is second only to lung cancer among all cancer-related deaths.¹ Most other developed countries are reporting similar probabilities for diagnosis and death. Breast cancer screening programs have been shown to decrease the mortality rates of women between ages 50 and 69,² since cancers are detected at an earlier, more easily cured stage. Conversely, the overall incidence of breast cancer is still rising, possibly owing to the increasing age of the population.³

Currently, imaging by X-ray mammography, ultrasound, and/or magnetic resonance imaging are the primary modalities⁴ used for breast imaging. These modalities use physical or chemical differences in tissue, such as the radiation attenuation coefficient, water content, or physical density, to observe differences in the tissue morphology that may suggest aberrant growth associated with cancer.

While the understanding of the mechanisms leading to breast cancer is increasing, they are still not fully understood, although it is apparent that the development of breast cancer is a slow process following initial transformation of the breast tissue.⁵ There is currently an effort within the research community to understand risk factors for the disease that are exhibited before or during this slow transformation process, but definitely prior to any clinical manifestation of breast cancer. This would enable members of the highest risk population to make educated decisions about increased screening and/or in-

Address all correspondence to Dr. Lothar Lilge, University of Toronto, 610 University Ave., Toronto, ON M5G 2M9, Canada. Tel: 416 946 4501 x 5743; E-mail: llilge@uhnres.utoronto.ca.

*Michelle K. Simick currently affiliated with Toronto Sunnybrook Regional Cancer Center, Toronto, Ontario, Canada.

†Roberta Jong currently affiliated with Sunnybrook and Women's College Health Sciences Center, Toronto, Ontario, Canada.

terventions to reduce risk. Risk factors are defined as those characteristics that are more common in people with the disease compared with the population at large.⁶ Risk factors related to breast cancer include age, country of residence, first-degree relatives or personal history of breast disease, genetic factors, anthropometric factors, menstrual and physiological factors all commonly combined into the Gail score,^{7,8} providing a numerical risk quantifier for the next decade or an individual's lifetime.

Although screening and risk reduction intervention have been shown to benefit the entire population at risk, for an individual member of the high-risk population, the risk-benefit ratio may not be favorable.⁹ To maximize the benefit for the individual as well, the relative risk quantifier employed is very large, so that most of the high-risk group members are identified while the quantifier minimizes the inclusion and hence exposure of low- or medium-risk subjects to potential side effects of the risk reduction interventions. Risk reduction interventions can be as benign as modifications to a subject's lifestyle, exercise, and diet, which has been shown to reduce the relative area of mammographic densities after 2 years,¹⁰ or they can be invasive, such as chemoprevention, including the use of tamoxifen,¹¹ aromatases,¹² and prophylactic mastectomy.¹³

Increased fibroglandular tissue in the breast that has a high X-ray attenuation coefficient, thus appearing bright in standard mammograms, is a known physiological risk factor.¹⁴⁻¹⁷ Areas appearing radiologically lucent represent fatty tissue of the breast that is rarely the source of aberrant growth. Radiologically opaque tissue is a common source of carcinomas, and consequently, the relative area of dense tissue is a strong risk factor. See Fig. 1 for examples of high and low X-ray dense breast tissue. Commonly, breast tissue density is quantified following breast cancer screening visits and it has been suggested that it can be affected by hormonal and dietary changes.¹⁸

Parenchymal density is used as the standard risk assessment tool¹⁴ in the study presented here because it provides the best available standard for risk in a cross-sectional study.

Breast tissue is a highly light-scattering medium and has relatively low absorption in the red and near infrared wavelength range, resulting in an adequate penetration depth of light. This allows a sufficient number of photons to be detected in a few seconds traversing through up to 7 cm of breast tissue while maintaining the incidence power below government guidelines for exposure of skin.¹⁹

Previous diagnostic studies of breast tissue showed that quantification of water, lipids, hemoglobin, and other tissue chromophores is feasible using near-infrared spectroscopy.²⁰ Fibroglandular tissue is expected to result in increased water and simultaneous decreased lipid-associated absorption, identifiable through absorption peaks at 978 and 930 nm, respectively²¹ (Fig. 2). It is also expected to have a higher scattering efficiency than adipose tissue, as seen in Fig. 3.¹⁸ Finally, hemoglobin (Hb) can be identified by an absorption peak at 760 nm, while oxygenated hemoglobin (HbO₂) has only a low and broad absorption, with a local maximum close to 920 nm.²¹

Transillumination spectroscopy has been shown to detect the presence of breast cancer.²² In this method, light emitted from the opposite side of the breast passes at least twice

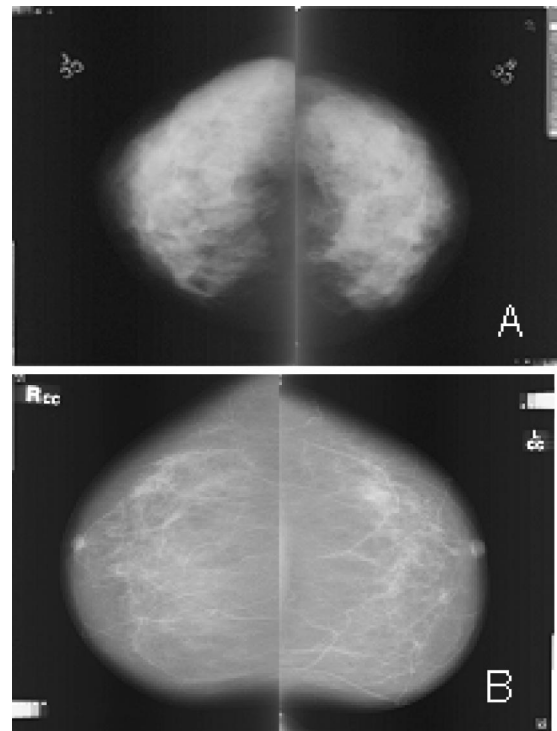


Fig. 1 Examples of X-ray-based mammograms showing breasts with either (a) high or (b) low tissue density. Note: Different X-ray exposures were used for the two examples.

through the skin. The skin's varying melanin content (depending on ethnicity and sun exposure) can affect the transmission spectrum, and hence may limit the predictive value of transillumination spectra because the melanin content does not affect breast cancer risk. While quantification of skin color is feasible based on diffuse reflectance spectroscopy,²³ and can permit subtraction of melanin-associated absorption, it was not done in this study, and participants were not stratified for skin color or ethnic background, in order to obtain densities and risk classifications that were independent of ethnicity.

Optical transillumination spectroscopy is not an imaging technique and thus only bulk tissue properties are obtainable and are characterized through spectral shape and intensity analysis. Hence, for comparison with mammographic-determined risk, the X-ray images were classified only as low, medium, or high tissue density, omitting spatial information about the density pattern.

This investigation was set up as a cross-sectional study to evaluate the feasibility of detecting and quantifying breast tissue density as an intermediate to risk prediction *in vivo* using visible and near-infrared transillumination spectroscopy. The hypothesis is that optical transillumination spectroscopy provides information consistent with conventional mammography in quantifying breast tissue density and hence, indirectly breast cancer risk, with an odds ratio comparable to that of mammography.

2 Methods

2.1 Instrumentation

The clinical spectrographic system, designed and built in-house, is shown as a schematic in Fig. 4. A 12-W halogen

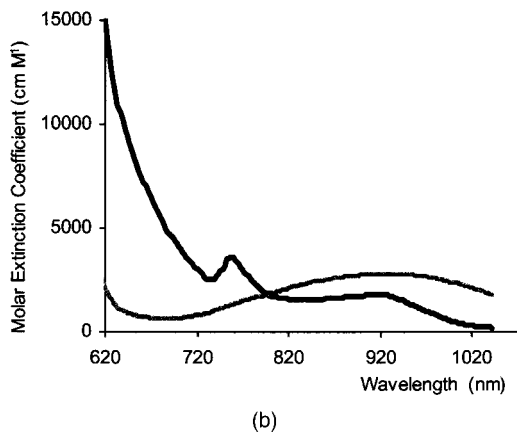
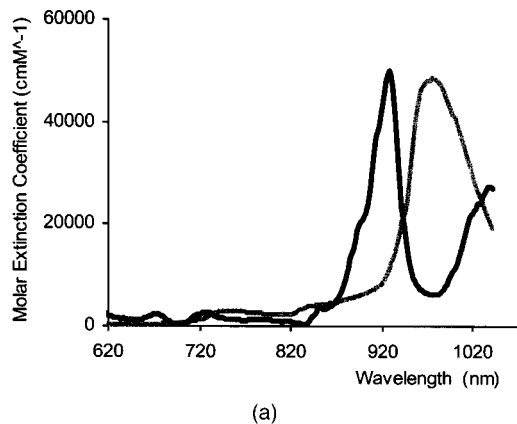


Fig. 2 Absorption spectra of some major chromophore constituents in breast tissue, including (a) water (gray) and lipid (black) and (b) hemoglobin (black) and oxygenated hemoglobin (gray).¹⁵

lamp (Welch Allyn, Buffalo, New York), with a stabilized power supply was used as the broadband light source. The ultraviolet, short-visible and midinfrared regions of the spectrum were blocked by a cutoff filter (<550 nm) and a heat rejection filter (KG4, Melles Griot, Carlsbad, Calif.), respectively. The remaining light in the 550 to 1300-nm range was coupled by a 20-mm focal length lens into a 5-mm diameter

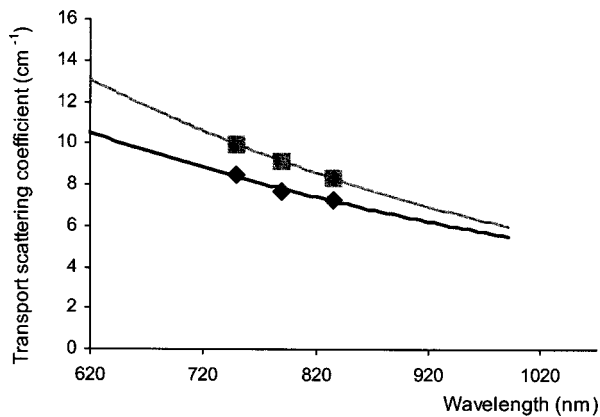


Fig. 3 Graph of the scattering coefficient (μ'_s) of adipose (black) and fibrous (gray) breast tissue in the wavelength range of interest. (Adapted according to Troy et al.¹¹).

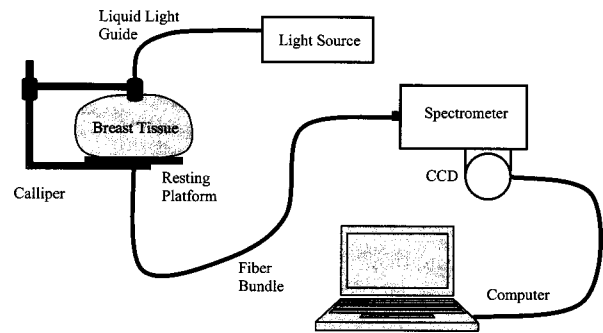


Fig. 4 Setup schematic of transmission measurement system, consisting of a continuous wave white light source, optodes (liquid light guide and fiber bundle in the caliper mount), breast support, spectrophotometer, and central processing unit.

liquid light guide (Kaiser Electronics, San Jose, Calif.), placed in contact with the top of the breast. The total radiant power delivered to the skin surface was <250 mW. The transmitted light was collected by a custom-made 7-mm diameter optical fiber bundle (P&P Optical Kitchener, Ontario, Canada) that was positioned coaxially with the source guide. The light guides were mounted in a caliper, the separation of which could be adjusted by hand so that both optodes were in contact with the breast. Contact of the source guide was firm, with the breast compressed locally by not more than 5 mm to ensure good coupling to the tissue. The holder for the source guide and the plate in which the detector guide was embedded were made of black plastic to model matched boundary conditions. During spectral measurements, the subject was seated and each breast in turn rested comfortably on a support plate, the height of which could be manually adjusted. No pretreatment of the skin surface was required.

The collected light was spectrally dispersed using a high-throughput holographic grating (15.7 lines/mm; Kaiser, Carlsbad, California) with a 0.5-mm entrance slit and detected with a 2-D, liquid nitrogen-cooled back thin silicon CCD array (F-125, Photometrics, New Jersey). The spectral resolution was <3 nm (FWHM) over the 625- to 1060-nm bandwidth. The peak quantum efficiency of the detector was >0.8 at 780 nm, falling to 0.2 at 1100 nm. The entrance slit of the spectrometer was imaged onto 50 rows of the CCD, thus increasing the dynamic range by over 25 fold. The dark count was ~0.06 electrons per hour. Further noise reduction was achieved using exposure times of 2 to 3 s and averaging up to 5 scans. The system's dynamic range was >5 OD (optical densities) with a signal-to-noise ratio of >10 to 10⁴ across the spectral range.

This study was approved under the institutional review boards of the University of Toronto and the University Health Network, with informed consent. Women were recruited through the Marvella Koffler Breast Center at Mount Sinai Hospital, Toronto. All had prior mammograms within 12 months of the spectral measurement, classified by a radiologist (RJ) as either low (<25%), medium (25 to 75%), or high (>75%) tissue density.¹⁴ Women showing large variations between both sides of the bilateral organ were not included in this analysis.

Table 1 Tissue density distribution for recruited volunteers and for population proportions from the National Breast Screening Study (ages 40 to 59).²¹

Density Category	Premenopausal			Postmenopausal			Total	Study Proportion (%)	Population Proportion (%)
	Training Set	Validation Set	Total	Training Set	Validation Set	Total			
Low	4	1	5	25	8	33	38	41	37
Medium	13	5	18	13	5	18	36	39	49
High	8	3	11	5	2	7	18	20	14

2.2 Measurement Procedure and Spectral Preprocessing

The total data acquisition time was approximately 15 minutes and was completed in complete darkness. A total of 8 spectra were collected per subject, representing medial, distal, lateral, and central quadrants of each breast. To date, a total of 92 women have been entered in the study, of whom 58 are postmenopausal. The wavelength dependence of the sensitivity was corrected daily by normalizing the transillumination spectra made through a standard consisting of 1-cm thickness, ultra-high density polyurethane (Gigahertz Optics, Munich, Germany), which has a very flat attenuation spectrum. All tissue spectra are given as optical density relative to this standard. Further preprocessing of spectra included correction for the tissue thickness by calculating the OD/cm at each wavelength. Autoscaling of the spectra, was done by normalizing the spectrum to the average spectrum off all spectra contained in the training set data for PCA model development (see later discussion), whereas spectra in the validation set were scaled using the same mean spectra. Principle component analysis requires random splitting of the dataset into a training set to iteratively optimize the algorithm and a training set to verify that the optimization can be generalized to all available spectra.

2.3 Data Analysis

The radiological classification produces a scalar quantity, namely the mammographic density, and the optical spectrum is a vector. Hence, only multivariate analysis techniques that are able to correlate vectors with scalars and that have been used extensively for different applications requiring the analysis of complex spectra, such as in chemometrics²⁴ and spectroscopic analysis in medical applications,^{25,26} were considered.^{27,28} Typically, these methods involve first a “training” step to identify the variance within a set of spectra and subsequently, a “prediction” or “validation” step to determine the accuracy of a separate set of spectra in predicting the outcome, which in this case is the tissue density classification. The specific analytical technique used here is Principal Components Analysis (PCA).

Mathematically, the PCA procedure is as follows. First, the spectral data are reduced in extent, while preserving the maximum amount of variance.²⁹ This is accomplished by solving for the covariance or correlation matrix of the data matrix $\mathbf{X}(m \times n)$ comprising all measured spectra ($n = 544$; training

set only) and the spectral range ($m = 436$ wavelengths), such that:

$$\text{cov}(\mathbf{X}) = \frac{\mathbf{X}^T \mathbf{X}}{n - 1} \quad (1)$$

PCA decomposes the data matrix \mathbf{X} as the sum of the outer products of the scalars of \mathbf{t}_i and vectors \mathbf{p}_i and a residual matrix \mathbf{E} :

$$\mathbf{X} = \mathbf{t}_1 \mathbf{p}_1^T + \mathbf{t}_2 \mathbf{p}_2^T + \mathbf{t}_3 \mathbf{p}_3^T + \dots + \mathbf{t}_i \mathbf{p}_i^T + \mathbf{E}$$

or

$$\mathbf{X} = \mathbf{TP}^T + \mathbf{E}, \quad (2)$$

where the elements of the \mathbf{t}_i ($n \times 1$) vectors are the scores that contain information on how the spectra relate to each other, and the \mathbf{p}_i vectors ($m \times 1$) or components are the eigenvectors of the covariance matrix that relate the selected variances to each other.

The scores (elements of \mathbf{t}_i) can be graphically plotted against one another to show clustering of related spectra. The PCA algorithm was trained on a test set ($n = 544$) and the same mathematical model, i.e., retaining the \mathbf{p}_i , was used to determine the scores \mathbf{t}_i on the validation set that consisted of the remaining $n_v = 192$ spectra.

The statistical significance for the PCA prediction was established using the high-density measure (HDM), which is defined as the ratio of spectra predicting a woman as having high mammographic density by the PCA algorithm compared with those categorized as having high tissue density by the radiologist. Conversely, the low-density measure (LDM) represents the ability to correctly identify those spectra that represent low tissue density. Hence, the HDM and LDM are similar to sensitivity and specificity, respectively.

3 Results

The dataset includes mammograms and spectral results from 92 subjects (aged 36 to 72 years). Fifty-eight women were postmenopausal, of whom 33 were classified as having low, 18 medium, and 7 high mammographic density. Of the 34 premenopausal women, 5, 18, and 11 were classified as having low, medium, and high density, respectively, as shown in Table 1. At present, this classification does not reflect the

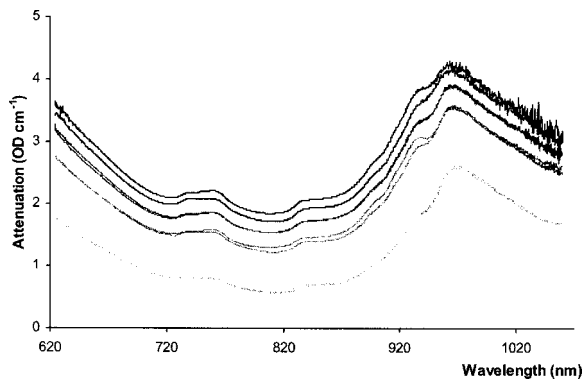


Fig. 5 Typical attenuation spectra from the four quadrants of both breasts in a volunteer. The spectra are corrected for the spectral system transfer function and tissue thickness. Note the good reproducibility between corresponding sides of the bilateral organ. Distal spectra show the lowest and the center position the highest attenuation.

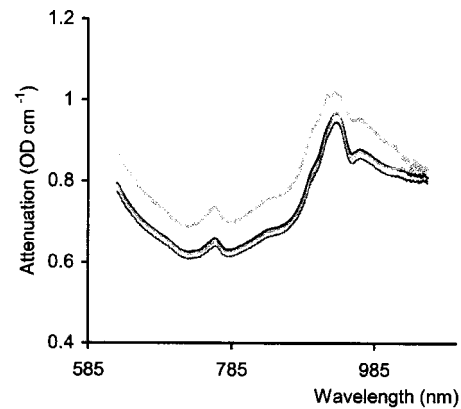
distribution observed in the general population during the Canadian National Breast Screening Study,¹⁵ but recruitment is continuing.

Figure 5 shows a typical set of measurements, consisting of 8 spectra from a single subject. Spectra from corresponding quadrants on each breast are very similar, a fact used by Egan and Dolan²² as a negative predictor for the absence of breast cancer.

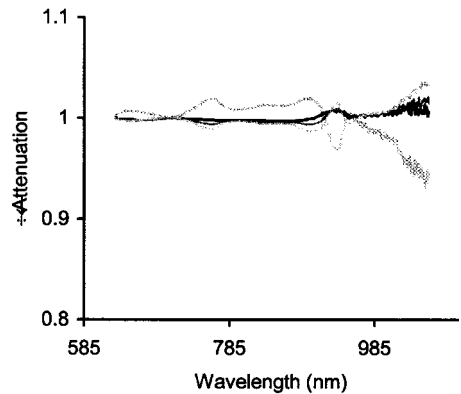
While transillumination is a local measurement, nevertheless a large volume of tissue is interrogated at each position (estimated as 25 cm³ for a 5-cm breast thickness). For positions close to the circumference of the breast boundary, losses will affect the overall intensity of the transmitted spectra and could influence the spectral shape; thus they could limit the predictive value of the transillumination technique. Hence, repeat measurements were made in one subject, starting at the center position and moving toward the medial position and beyond toward the circumference of the breast. The resulting transillumination spectra are shown in Fig. 6, indicating that the overall absorbance is wavelength independent up to a distance of 1 cm from the circumference of the breast, where the losses increase and become wavelength dependent. Thus, measurements were taken at least 1 cm from the circumference of the breast.

The reproducibility of the optical transillumination measurements was analyzed by repeat procedures on one subject during visits over a period of 18 months. Figure 7 shows the correlation of the t_1 and t_2 scores from two of the repeat spectra. Component scores (t_1 and t_2) vary between quadrants, but cluster tightly for a given position, indicating that the spectroscopy data are reproducible. Figure 8 shows the reconstruction of a randomly selected transillumination spectrum, according to the variance captured only by p_1 and p_2 , as well as that captured by the first four components in thickness-corrected spectra. The reconstruction from all four components shows a good representation.

Figure 9(a) shows the principal components (p_i) resulting from PCA using $n = 544$ corrected spectra. p_1 to p_4 represent, respectively, 97.6, 1.2, 0.6, and 0.3% of the variance in the total dataset, for a combined 99.8% of the variance. While all density classes were employed for PCA training, the resulting



(a)



(b)

Fig. 6 Effect of boundary losses at the breast circumference. (a) Attenuation spectra from a volunteer at various distances from the breast circumference (center position black, medial position dark gray), 2 cm from circumference (gray), and 1 cm from circumference (light gray). (b) Ratio of the same spectra over the average of all four spectra to exaggerate spectral variance that is due to boundary losses.

cluster plot of the scores for t_1 and t_2 as shown in Fig. 10(a) present data for the low and high tissue density classes only, which is similar to mammography-derived tissue densities. The odds ratio for risk is calculated based on the difference of these two extreme classes. Here the cluster plot shows discrimination of the breast tissue density across a diagonal line in the t_1 versus t_2 space. Based on a physiological interpretation of the information carried by the principal components, p_1 and p_2 quadrants indicating scattering power and relative water to lipid ratios are indicated.

Spectra that had not been corrected for thickness were used to determine the effect of thickness on the shape of the component vectors p_1 to p_4 [Fig. 9(b)] and the resulting cluster plots of t_1 versus t_2 [see Fig. 10(b)]. The component spectra are almost identical to the thickness-corrected components, whereas the cluster plots of t_1 versus t_2 show discrimination as a function of t_2 only. The reproducibility of the principle components between thickness-corrected and uncorrected spectra indicates the general validity of the approach to using thickness-corrected spectra in this PCA analysis.

Plotting of t_3 versus t_4 or other combinations of the scores resulted in poor separation of the low- and high-density clusters (data not shown) and were not further pursued. Similarly,

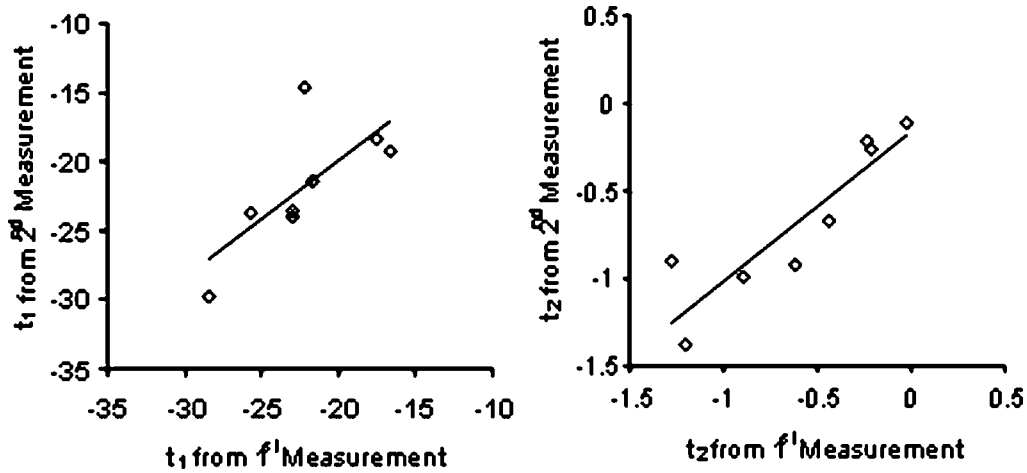


Fig. 7 Repeatability of t_1 and t_2 in one volunteer at all 8 positions. The slope of the regression line is 1.03 and 0.87, and the Pearson correlation coefficient is 0.72 and 0.84 for t_1 and t_2 , respectively.

component spectra and cluster plots were obtained also for autoscaled and transfer function-corrected spectra (data not shown). The resulting HDM and LDM values for the different spectral preprocessing methods are shown in Table 2. The symmetry across the same bilateral quadrants for each individual is shown in Fig. 11 for all scores of t_1 and t_2 derived from thickness-corrected spectra, reflecting a pool of women with homogeneous density distribution across both breasts.

4 Discussion

Bilateral symmetry in the spectra at corresponding quadrants (Fig. 11) is expected in our study population since it is a criterion for determining the absence of breast cancer according to previous studies by Egan and Dolan.²²

Autoscaling of the spectra prior to PCA modeling removes some spectral information since the subtracted mean spectrum is wavelength dependent. Since the spectral features contributing to the discrimination between high and low breast density or risk are not known, losing spectral information is not advisable, even though no significant loss in HDM and LDM was noted. In addition, calculating component spectra after

autoscaling will not allow the use of principal components filters in future work, as suggested elsewhere.³⁰

Cluster plots [Fig. 10(a)] based on the scores t_1 and t_2 resulting from thickness-corrected spectra demonstrated that it is possible to differentiate between subjects having low or high breast tissue densities, which is the basis of determining the odds ratio for cancer risk based on mammographic density.¹⁵ Adding the medium density class into the HDM and LDM will not change the former, but will lower the latter by 0.2 to 0.3, depending on the actual model used.

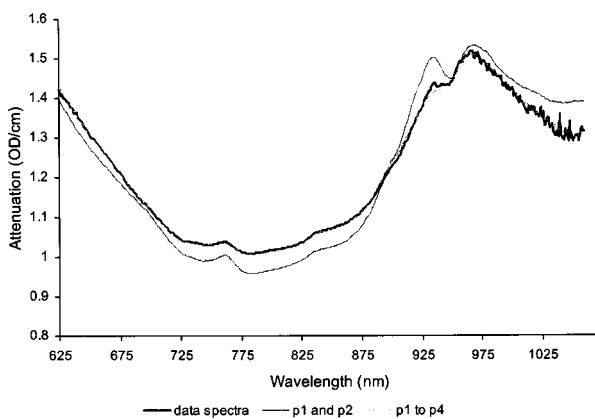


Fig. 8 Raw data spectrum (black) and reconstruction using either only the first two components (light gray) or the first four components (gray) based on the principal components shown in Fig. 9(a).

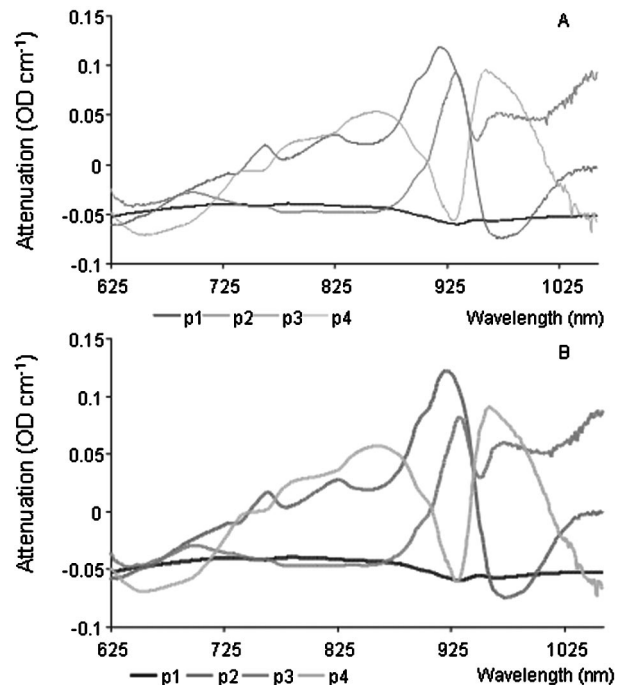


Fig. 9 Plot of components p_1 to p_4 (black to light gray, respectively) from PCA using (a) tissue thickness and spectral transfer function-corrected spectra and (b) only spectral transfer function-corrected spectra (derived from 92 volunteers).

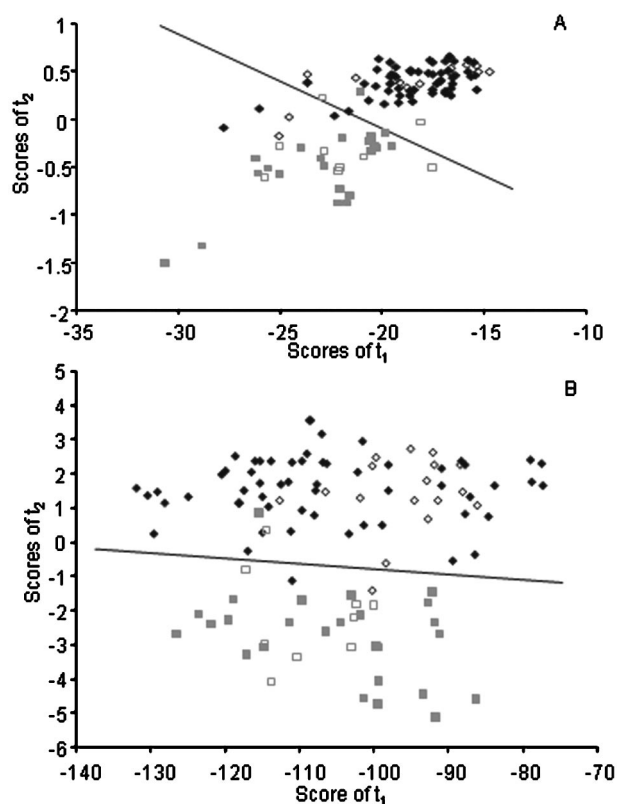


Fig. 10 Cluster plot of t_1 versus t_2 resulting from PCA using (a) thickness and system spectral transfer function-corrected spectra and (b) only spectral transfer function-corrected spectra from volunteers with high (square) or low (diamond) breast tissue density. Only scores for the center measurements are shown, with the training spectra shown as closed and the validation spectra as open symbols. (a) also includes a physiological interpretation of the data points within the t_1 versus t_2 space.

While PCA models for both native and thickness-corrected spectra enable differentiation between high and low breast tissue densities, their t_1 versus t_2 cluster plots differ. In the model based on native nonthickness-corrected data, p_1 cannot

Table 2 High-density and low-density measures (HDM and LDM) of principal component analysis results for test and validation set measurements.

	Test Set		Validation Set	
	HDM	LDM	HDM	LDM
Data preprocessing				
Transfer function-corrected (Fig. 9b)	84.6%	97.0%	87.5%	90.3%
Thickness and transfer function-corrected (Fig. 9a)	88.4%	93.1%	92.5%	88.8%
Autoscaled—transfer function-corrected (data not shown)	85.6%	94.4%	90.0%	86.1%
Autoscaled—thickness and transfer function-corrected (data not shown)	86.5%	91.8%	92.5%	90.3%

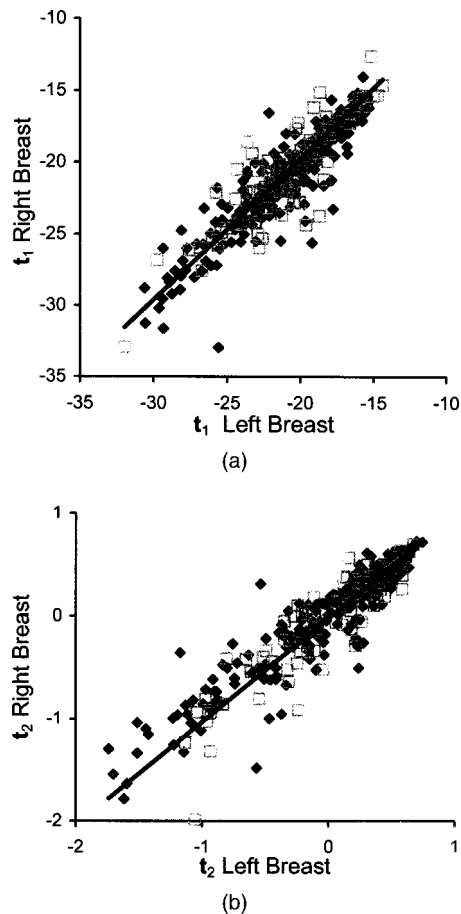


Fig. 11 Comparison of the (a) t_1 and (b) t_2 scores for all quadrants of the left versus those of the right breasts in volunteers with either high or low tissue density. Black diamonds represent volunteers from the training set; gray squares represent those from the validation set. Slope and Pearson correlation coefficient are 0.94 and 0.76 for t_1 and 1 and 0.83 for t_2 , respectively.

differentiate between high- and low-density tissue. The range of t_1 values is smaller in the thickness-corrected data, as seen in Fig. 10(a), compared with the nonthickness-corrected data in Fig. 10(b). This is possibly due to the variance added by the thickness of the physical tissue to the variance in the spectral dataset introduced. This indicates that the thickness values contribute to the magnitude of p_1 , masking other contributions that could differentiate between tissue densities, such as light scattering, and thus leaving only t_2 to preserve information distinguishing between the two groups of breast tissue density. Principal component spectra one (p_1) based on the thickness-corrected spectra is de facto wavelength independent, but includes losses that are due to the optical path length (and therefore light scattering) and losses at the circumference of the breast. The t_1 range of the low tissue density cluster relative to that of the high-density cluster between the PCA models based on either the raw spectra or the thickness-corrected data most likely reflects the fact that p_2 carries only approximately 1% of the total variance seen in the dataset. Preprocessing of the spectra, including thickness correction, is clinically relevant since it is controllable and it has been shown that thickness will contribute nonuniformly to the

spectra, owing to the correlation between lower density and larger breasts.¹⁴

When the autoscaled and nonautoscaled data were compared, there were minimal changes in the principal component spectra and minor differences in HDM and LDM values; see Table 2. Autoscaling as part of the preprocessing can degrade regions with flat or extreme spectral variation.²⁸ Here, degraded spectral features could include regions of the spectrum with minimal wavelength dependence and hence, a first derivative close to zero. For example, the hemoglobin inflection points are more pronounced in the non-autoscaled data than in the autoscaled components. Conversely, the spectral features of water and lipids are large compared with other structures in the spectra, but are less pronounced after auto scaling. In this study, the only difference in the performance of the model is in the training set using non-autoscaled spectra having about 2% higher scores for both HDM and LDM.

Principal components can reveal particular regions of the spectrum that represent important physical properties or entities within the tissue that contribute to differentiation. Component spectra \mathbf{p}_1 and \mathbf{p}_2 are the most important and cover the highest amount of variance in the dataset. While components 3 and 4 have shapes similar or inverse to that of component 2, they take less variance into account.

The derivation of OD used here, which is based on a wavelength-dependent transfer function calibration using a polyurethane block with high Mie scattering, resulted in the surprisingly flat spectral shape of the principal component spectra \mathbf{p}_1 because the wavelength-dependent Mie scattering cancels when the ratio of the two spectra is taken. Hence, \mathbf{p}_1 carries optical scattering information despite not showing the typical λ^{-1} dependence,³¹ and thus the inverse of \mathbf{t}_1 represents the overall scattering power. Low-density tissue spectra have a reduced amount of scattering compared with high-density tissue, and therefore have higher values of \mathbf{t}_1 , as seen in Fig. 10(a). This relationship in scattering properties is also seen in the scattering coefficient data by Peters et al.³² and Troy et al.¹⁸

Component vector \mathbf{p}_2 , makes differentiation between low and high tissue densities possible through its spectral features related to the lipid, with inverse water peaks present at 930 and 980 nm, respectively. Thus, when \mathbf{t}_2 is positive, the lipid-associated attenuation is the dominant feature, as anticipated for fatty or low-density tissue. Spectra from the high-density tissue have a negative \mathbf{t}_2 , and water absorption becomes the dominant structure in the component spectrum. Graham et al.³³ also observed this relationship between water and density values when they used magnetic resonance imaging (MRI) to quantify percent density. In their study, the water content of the tissue was measured directly and showed adequate correlation to percent tissue density ($r=0.79$).

Contributions by hemoglobin to the spectral features of \mathbf{p}_2 are observed between 625 and 850 nm, where the negative slope and inflection points of the hemoglobin curve are apparent. Dense breast tissue has lower \mathbf{t}_2 scores than low-density tissue, indicating higher hemoglobin and water contributions. Conversely, \mathbf{p}_3 shows a lipid absorption peak, but water and hemoglobin absorption are absent. Hence, if it is used as a third discriminator, the overall content of fatty tissue is represented. The simultaneous appearance of water and hemoglobin absorption in \mathbf{p}_2 can be explained physiologically, because

tissues with higher water content and hence cellular content, require improved vascular supply and thus have an increased blood volume.³⁴ Since positive \mathbf{t}_2 scores are related to low tissue density and positive \mathbf{t}_1 scores are related to low tissue scatter, the cluster plot of \mathbf{t}_1 and \mathbf{t}_2 can be divided into quadrants as shown in Fig. 10(a), highlighting the relationship between the spectral features and the known physical attributes of breast tissue.

While cluster plots based on \mathbf{t}_3 and \mathbf{t}_4 do not allow good differentiation between high- and low-density tissue, regions of the corresponding component spectra \mathbf{p}_3 and \mathbf{p}_4 show interesting effects. For example, for \mathbf{p}_3 there is a red-shifted lipid peak and a small blue-shifted water peak, and \mathbf{p}_4 shows influence from both forms of hemoglobin, with the same slope as \mathbf{p}_2 but inverse inflection points. The underlying physical or physiological effects for these observations are unclear at this time. While the amplitudes and general shape of the spectra are similar to \mathbf{p}_2 , the magnitude of the scores for \mathbf{t}_3 and \mathbf{t}_4 are much smaller than those of the first two components, and may represent only relative corrections for \mathbf{p}_2 .

5 Conclusions

In vivo optical transillumination spectroscopy is technically feasible and capable of predicting breast tissue densities with good correlation to mammographic densities. Since it has good potential to be developed into a preferred method of assessing cancer risk, the strength of a direct correlation with risk needs to be proved in a case-control study and possibly also a longitudinal study to estimate the validity of the correlation and its predictive value for a longer period of time.

According to the results of the current study, it is anticipated that the odds ratio of the transillumination measurements should be close to those of the parenchymal densities seen on mammograms (i.e., between 4 and 6), since the PCA results show HDM and LDM values close to or above 0.90.

Transillumination spectroscopy may offer a novel “first step” in the risk assessment of healthy women regardless of age, menstrual cycle, ethnic background, or menopausal status because the data and analysis presented here were not subject to stratification by three factors. Indeed the HDM and LDM did not improve when stratifications based on menstrual cycle, skin color, or menopausal status were introduced.

Spectral features associated with predicting tissue density include water and lipids, as well as spectral features related to hemoglobin absorption. The effect of light scattering on measured spectra is important in the differentiation of breast tissue density after correction of the data for tissue thickness.

At this stage, HDM and LDM values close to or above 90% are very promising as a way of distinguishing between low- and high-density tissues because they are higher than those obtained with other physical examinations, such as ultrasound³⁵ and magnetic resonance imaging,³³ which are reported to be between 70 and 80%.

Optical transillumination spectroscopy offers the potential of a real-time and cost-effective method with the ability of the current instrument to classify tissue densities for breasts that are up to 7 cm in thickness. Improvements in CCD technology, such as deep-depletion wells, can increase the optoelectronic detection and thus will increase the detection ability. An added advantage of transillumination spectroscopy over ultra-

sound and MRI is the fact that results are derived from preset mathematical models and hence no additional trained personnel is required for image interpretation or assessment. This reduces the overall cost to the health-care system for this risk assessment technique. The compactness of the devices makes them highly mobile and ideal for serving remote areas or developing countries. The painless procedure and the inherent safety of this method will most likely contribute to a higher compliance rate, thus possibly assisting in influencing overall survival rates.

One notable limitation in this preliminary study was the number of study subjects, which may have resulted in suboptimal predicted values for HDM and LDM. Also, by using cluster analysis in 3-D or higher dimensions, other components such as p_4 can be included to improve classification of tissue density.

X-ray mammography uses ionizing radiation and is considered unacceptable as a tool to assess breast density for women less than 40 years of age and for frequent measurement, whereas transillumination spectroscopy is safe for women of all ages. This allows risk assessment to begin at a much younger age, when the lifestyle and diet are perhaps easier to influence. Having one to two decades more to effectively reduce the cancer risk makes these mild risk reduction interventions a valid option for women while possibly also leading to reduced incidence.

While optical transillumination spectroscopy may be a promising tool to monitor the effectiveness of risk reduction interventions such as chemopreventive, dietary, or lifestyle changes aimed at reducing breast cancer risk, its ability to detect physical changes over a period of time in the breast tissue of a given individual needs to be demonstrated in a prospective longitudinal study.

Acknowledgment

The authors wish to thank Dr. Robert Weersink for assistance in developing the specific PCA models, and Ms. Samantha Dick for assistance in patient accrual and database maintenance. This work was funded under contract DAMD17-00-1-0393 from the U.S. Army Medical Research and Material Command.

References

- National Cancer Institute of Canada, *Canadian Cancer Statistics 2001*, Toronto Canada (2001).
- National Cancer Institute of Canada, *Canadian Cancer Statistics 2000*, Toronto, Canada (2000).
- National Cancer Institute of Canada, *Canadian Cancer Statistics 1997*, Toronto, Canada (1997).
- E. Paci, S. Duffy, and M. Rosseli di Truco, "11.3 Mammographic screening: from the scientific evidence to practice," in *The Oxford Textbook of Oncology*, Oxford University Press, New York (2000).
- L. E. Janocko, K. A. Brown, C. A. Smith, L. P. Gu, A. A. Pollice, S. G. Singh, T. Julian, N. Wolmark, L. Sweeney, J. F. Silverman, and S. S. Shackney, "Distinctive patterns of Her-2/Neu, c-myc and Cyclin D1 gene amplification by fluorescence in situ hybridization in primary human breast cancers," *Cytometry* **46**, 136–149 (2001).
- J. Byng, *Mammographic Densities and Risk of Breast Cancer*, University of Toronto Press, Canada (2000).
- J. P. Costantino and M. H. Gail, "Validation studies for models projecting the risk of invasive and total breast cancer incidence," *J. Natl. Cancer Inst.* **91**, 1541 (1999).
- A. Schatzkin and M. Gail, "The promise and peril of surrogate end points in cancer research," *Natl. Rev. Cancer* **2**, 19–27 (2002).
- A. N. Freedman, B. I. Graubard, S. R. Rao, W. McCaskill-Stevens, R. Ballard-Barbash, and M. H. Gail, "Estimates of the number of US women who could benefit from tamoxifen for breast cancer chemoprevention," *J. Natl. Cancer Inst.* **95**, 526–532 (2003).
- N. F. Boyd, C. Greenberg, G. Lockwood, L. Little, L. Martin, J. Byng, M. Yaffe, and D. Tritchler, "Effects at two years of a low-fat, high carbohydrate diet on radiologic features of the breast: results from a randomized trial," *J. Natl. Cancer Inst.* **89**, 488–496 (1997).
- O. Konec, M. Goyal, and R. E. Reaven, "Can tamoxifen cause a significant mammographic density change in breast parenchyma?" *J. Clin. Imag.* **25**, 303–308 (2001).
- J. N. Ingle, "Aromatase inhibition and anti estrogen therapy in early breast cancer treatment and chemoprevention," *Oncology* **15**, 28–39 (2001).
- S. Taucher, M. Gnant, and R. Jakesz, "Preventive mastectomy in patients at breast cancer risk due to genetic alterations in the BRCA1 and BRCA2 gene," *Cur. Concepts Clin. Surg.* **388**, 3–8 (2003).
- N. F. Boyd, G. A. Lockwood, J. Byng, D. L. Tritchler, and M. Yaffe, "Mammographic densities and breast cancer risk," *Cancer Epidemiol. Biomarkers Prevent.* **7**, 1133–1144 (1998).
- N. F. Boyd, J. W. Byng, R. A. Jong, E. K. Fishell, L. E. Little, A. B. Miller, G. A. Lockwood, D. L. Tritchler, and M. J. Yaffe, "Quantitative classification of mammographic densities and breast cancer risk: results from the Canadian National Breast Screening Study," *J. Natl. Cancer Inst.* **87**, 670–675 (1995).
- M. Freedman, J. San Martin, J. O'Gorman, S. Eckert, M. E. Lippman, S. C. B. Lo, E. L. Walls, and J. C. Zeng, "Digitized mammography: a clinical trial of postmenopausal women randomly assigned to receive raloxifene, estrogen, or placebo," *J. Natl. Cancer Inst.* **93**, 51–56 (2001).
- J. Wolfe, "Risk for breast cancer development determined by mammographic parenchymal pattern," *Cancer* **37**, 2486–2492 (1976).
- T. Troy, D. L. Page, and E. M. Sevick-Muraca, "Optical properties of normal and diseased breast tissues: prognosis for optical mammography," *Biomed. Opt. Spectroscopy. Diagnos.* **3**, 59–66 (1996).
- International Electrotechnical Commission, *Group Safety of Laser Products Part 1: Equipment Classification, Requirements and User's Guide*, IEC, Geneva (1993).
- V. Quaresima, S. J. Matcher, and M. Ferrari, "Identification and quantification of intrinsic optical contrast for near-infrared mammography," *Photochem. Photobiol.* **67**, 4–14 (1998).
- A. J. Welch and M. J. C. van Gemert, Eds., *Optical-Thermal Response of Laser-Irradiated Tissue*, Plenum, New York (1995).
- R. L. Egan and P. D. Dolan, "Optical spectroscopy. Pre-mammography marker," *Acta Radiol.* **29**, 497–503 (1988).
- R. A. Weersink, L. D. Marret, and L. Lilje, "Validation of self-reported skin colour via principal component analysis of diffuse reflectance spectra of the skin," *Proc. SPIE* **3917**, 232–237 (2000).
- L. Chen, W. Chew, and M. Garland, "Spectral pattern recognition of in situ FT-IR spectroscopic reaction data using minimization of entropy and spectral similarity (MESS): application to the homogeneous rhodium-catalyzed hydroformylation of isoprene," *Appl. Spectrosc.* **57**, 491–498 (2003).
- A. Henrich, P. Hoffmann, H. M. Ortner, T. Greve, and H. Itzel, "Non-invasive identification of chemical compounds by energy dispersive X-ray fluorescence spectrometry, combined with chemometric methods of data evaluation," *Fresenius' J. Anal. Chem.* **368**, 130–138 (2000).
- S. Sukuta and R. Bruch, "Factor analysis of cancer Fourier transform infrared evanescent wave fiberoptical (FTIR-FEW) spectra," *Lasers Surg. Med.* **24**, 382–388 (1999).
- D. M. Haaland and E. V. Thomas, "Partial least-squares methods for spectral analysis. 1. Relation to other quantitative calibration methods and the extraction of qualitative information," *Anal. Chem.* **60**, 1193–1202 (1988).
- D. M. Haaland and E. V. Thomas, "Partial least-squares methods for spectral analysis. 2. Application to simulated and glass spectral data," *Anal. Chem.* **60**, 1202–1208 (1988).
- B. M. Wise, *PLS Toolbox Tutorial: Matlab Version 6*, Eigenvector Research Inc., Seattle, WA (2000).
- J. N. Y. Qu, H. P. Chang, and S. M. Xiong, "Fluorescence spectral imaging for characterization of tissue based on multivariate statistical analysis," *J. Opt. Soc. Am. A* **19**, 1823–1831 (2002).
- R. Cubeddu, C. D'Andrea, A. Pifferi, P. Toroni, A. Torricelli and G. Volentini "Effects of the menstrual cycle on the red and near-infrared

- optical properties of the human breast," *Photochem. Photobiol.* **72**, 383–391 (2000).
32. V. G. Peters, D. R. Wyman, M. S. Patterson, and G. L. Frank, "Optical properties of normal and diseased human breast tissues in the visible and near infrared," *Phys. Med. Biol.* **35**, 1317–1334 (1990).
 33. S. J. Graham, M. J. Bronskill, J. W. Byng, M. J. Yaffe, and N. F. Boyd, "Quantitative correlation of breast tissue parameters using magnetic resonance and X-ray mammography," *Br. J. Cancer* **73**, 162–168 (1996).
 34. J. W. Byng, J. P. Critten, and M. J. Yaffe, "Thickness-equalization processing for mammographic images," *Radiology* **203**, 564–568 (1997).
 35. L. Kaizer, E. K. Fishell, J. W. Hunt, F. S. Foster, and N. F. Boyd, "Ultrasonographically defined parenchymal patterns of the breast: relationship to mammographic patterns and other risk factors for breast cancer," *Br. J. Radiol.* **61**, 118–124 (1988).